Proceedings of the 4th WSEAS Int. Conf. on HEAT TRANSFER, THERMAL ENGINEERING and ENVIRONMENT, Elounda, Greece, August 21-23, 2006 (pp305-310)

# Study and analysis of the influence of a small heating source position on the natural convective heat transfer in a square cavity

MASSIMO PARONCINI, FRANCESCO CORVARO, MARIA MADDALENA DE PADOVA
Dipartimento di Energetica
Università Politecnica delle Marche
Via Brecce Bianche, 60100, Ancona
ITALY

*Abstract:* - In this paper it is investigated the influence of a small heating source position in the bottom of the square cavity. The analysis was conducted with an experimental study with real-time and double-exposure holographic interferometry, which was compared with numerical analysis.
The results of the comparison was shown in Ra-Nu graph for both two configuration of the heat strip in the square cavity.

*Key-Words:* - Natural convection; Square enclosures, Holographic interferometry; Numerical investigation.

## Nomenclature

d position of the heat source (m)
g modulus of the gravity vector (g=9.81 m $s^{-2}$)
H square cavity side (m)
k thermal conductivity (W $m^{-1}$ $K^{-1}$)
l heat source length (m)
L cavity depth in the experimental tests (m)
Pr $\frac{\upsilon}{\alpha}$ Prandl number
$Nu_h$ local Nusselt number
$\overline{Nu}_h$ average Nusselt number on the heat source
Ra $\frac{g\beta H^3 (T_h - T_c)}{\upsilon\alpha}$ Rayleigh number
T temperature (K)
T $\frac{(T_h + T_c)}{2}$ average temperature (K)
ΔT (Th - Tc) temperature difference between heat source and cold plate (K)
x, y Cartesian coordinate
X,Y $\frac{x}{H}, \frac{y}{H}$ dimensionless Cartesian coordinate

Greek Letters

β thermal expansion coefficient ($K^{-1}$)
δ $\frac{(d + \frac{l}{2})}{H}$ dimensionless position of the heat source
ε $\frac{l}{H}$ dimensionless length of the heat source
θ $\frac{(T - T_c)}{(T_h - T_c)}$ dimensionless temperature
υ kinematic viscosity ($m^2$ $s^{-1}$)
ρ density (kg $m^{-3}$)

Subscripts

c cold wall
h hot wall

## 1 Introduction

The natural convection in a square cavity has a very interesting role in a lot of engineering applications, such as solar energy system, cooling of the electronic circuits, conditioning of the air and many others, therefore it has an important role in the applied research.
Technical literature presents so many study on natural convection in square cavity and many of this study analyze convective phenomenon by numerical simulation.
Valencia and Frederick [1] elaborated a numerical investigation about the heat transfer of air in square cavities with partially active vertical walls.
Aydin el al. [2] simulated numerically the natural convective heat transfer in air in a square cavity cooled from the side walls and heated by a strip placed at the center of bottom wall.
Nibarufata et al. [3] investigated numerically the natural convection in partitioned enclosures with localized heating from below.
Ramos and Milanez's [4] paper treats the natural convection in cavities heated from below by a thermal source, which dissipated energy at a constant rate.
In this paper the cavity testing is a square enclosure and it is analyzed the influence of the position of the

heat stripe, placed on the bottom of the cavity, on natural convection heat transfer.
The cavity is, at the same time, cooled from the side walls and it's filled with air.
The temperature distribution is investigated experimentally by the real-time and double-exposure holographic interferometry, for analyzing temporary and stationary evolution.
The experimental results were compared with the results of the numerical analyses and shown in Nu-Ra graph for both two positions of the heat source, for Ra from $1 \cdot 10^5$ to $3 \cdot 10^5$ in experimental analysis and for Ra from $1 \cdot 10^5 < Ra < 3 \cdot 10^5$ in numerical simulation.

## 2 Experimental apparatus

The main components of the experimental apparatus, rappresented in Fig.1, include the test cell, filled with air at atmospheric pressure, the pneumatic auto-levelling table, the holographic interferometry, three thermostatic baths and the data acquisition system.

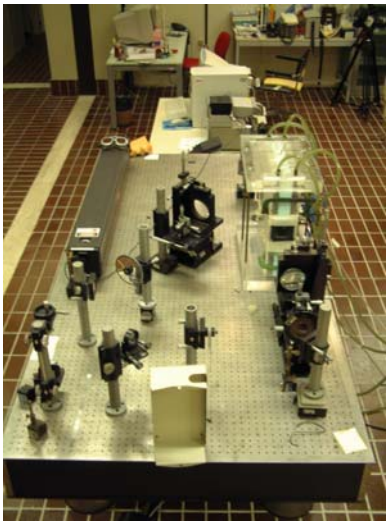

Fig.1 Experimental apparatus

The test-cell, shown in Fig.2, has a square transversal section of H=0,05 m. The brass heat source is positioned on the lower horizontal wall and it has a temperature $T_h$, maintained constant through the continuous circulation of thermostatic fluid.
The lateral vertical walls, made of aluminum, are cooled at a uniform temperature Tc by a fluid which is cooled by two other thermostatic baths.
The end vertical walls are made of glass to permit the access of the laser beam

The top and the bottom surfaces of the enclosure are made up of Plexiglas and can be expected adiabatic.
The test-cell dimension along the longitudinal direction is 0,41 m, it is greater than H enough to permit that air motion develop along z axis, parallel to the laser beam, allowing to neglect the end effect and to consider the problem as two-dimensional problem.
The components temperature of the test-cell is measured with copper-constantan thermocouples.
Ten thermocouples are positioned on the surfaces of the cool lateral walls and three on the brass surface of the heat source.
The last one is positioned in the top part of the cavity and it is a temperature reference for the evaluation of the interferograms. The difference among the three values of the temperature on the brass plate is less than 0,1 K therefore the situation can be considered isotherm, on the lateral wall the maximum difference among the five thermocouples is 0,5 K.

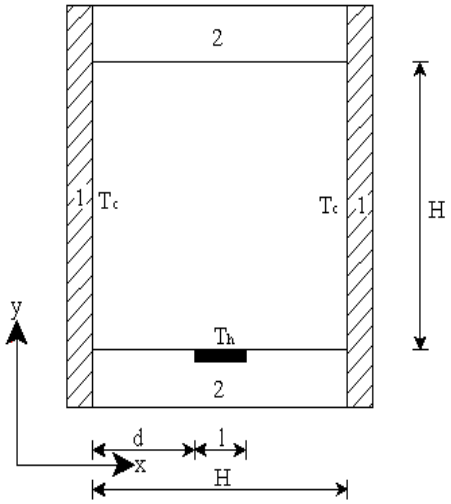


Fig.2

The light source is an Argon-Ion laser with a nominal power rating of 4 W, with Etalon for the 514,5 nm wave length.
Both object and reference beams have a maximum diameter of 0,15 m.
The investigation of steady-state convective heat transfer is studied with the double-exposure holographic interferometry technique, the temporal evolution is investigated with the real-time technique, that allow us to observe the presence of plume oscillations.
The Rayleigh numbers investigated changes from $1 \cdot 10^5$ to $3 \cdot 10^5$.
The paper wants to analyze the change caused on the heat convective flow by the two different

positions of the heat source in the bottom side of enclosure (d=0,012 m and d=0,015); in the analysis the dimension of the heat brass source is ε=1/5 of the side of the cavity.
The local Nusselt number on the heat source at the location x is calculated with the expression:

$$Nu(x) = -\frac{\partial\theta}{\partial y}\bigg|_{y=0} \quad (1)$$

The average Nusselt number on the heat stripe $\overline{Nu}_h$ is calculated by:

$$\overline{Nu} = \frac{1}{\varepsilon}\int_{\delta-\frac{\varepsilon}{2}}^{\delta+\frac{\varepsilon}{2}} \mathrm{Nu(x)}dx \quad (2)$$

where the dimensionless parameters introduced are:

$$X = \frac{\mathrm{x}}{H};\ Y = \frac{y}{H};\ \vartheta = \frac{T-Tc}{Th-Tc};\ \varepsilon = \frac{l}{H};\ \delta = \frac{d+\frac{l}{2}}{H}. \quad (3)$$

## 3 Numerical procedure and setting

The numerical simulation is developed with a finite volume code Fluent 6.0 using the Boussinesq approximation for air.
The numerical results are carried out with the segregated solvers [7] for $1\cdot10^5 < Ra < 3\cdot10^5$.
In the analysis by the software the cavity was reproduced with the real dimensions, and the temperature is assegned to the lateral walls and to the heated strip till to obtain the analyzed Rayleigh number as in the experimental analysis. The other surfaces are assumed adiabatic as in the experimental analysis.
The model was composed of a uniform mesh of square cells and a number of the mesh cells is 25000 so that it produce a valid results, with processing time not too high.
The calculation starts with the steady solvers where the dimensionless time steps range from $10^{-4}$ to $10^{-6}$, while the number of the time steps has been chosen sufficiently high to have an asymptotic steady-state solution.
The unsteady procedure permits the analysis of possible periodicities, of instabilities in the motion; the maximum number of interations per time stem is generally high enough to reach the grid limit of calculation with a value for convergence of $10^{-13}$.
The numerical average Nusselt number ( $\overline{Nu}$ ) on the heating element is calculated with:

$$\overline{Nu} = \frac{\frac{q_{tot}}{A_h}}{k\cdot\frac{\Delta T}{l}} \quad (8)$$

Where $q_{tot}$ is calculated with the software, $A_h$ is the heater surface and $K(W\cdot M^{-1}\cdot K^{-1})$ is the thermal conductivity of air evaluated at the heating stripe temperature.
The numerical local Nusselt number (Nu), referred to the heat source is:

$$Nu = \frac{q''}{k\cdot\frac{\Delta T}{l}} \quad (9)$$

where q" is the heat flux density ($W/m^2$), computed by the Fluent on each cell of the mesh.

## 4 Results and discussion

The temporal evolution of the convective motion was investigated with the real-time holographic interferometry, some frames of recording are represented in Fig.3 for the second case studied with heat source having a side positioned in the middle of the enclosures (δ=0,4).
In Fig.3a it is visible the first instant of the flow while the Fig. 3b shows a first development of convective heat transfer.

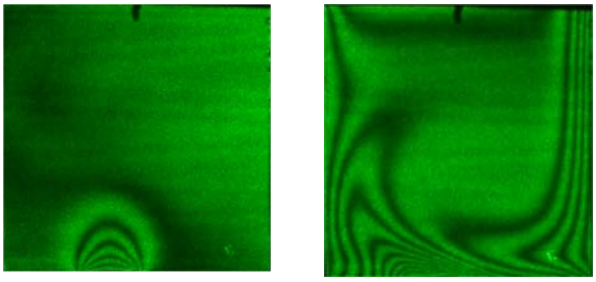

a) δ=0.4;t=19s; Ra=$1.39\cdot10^5$ b) δ=0.4;t=128s; Ra=$1.7\cdot10^5$

Fig.3 Real Time Interferograms

In the Fig.4 and in Fig.5 are visible the double exposure interferogram for both two configuration (δ=0,5 and δ=0,4).

a) Ra=$1.33\cdot10^5$ a) Ra=$1.38\cdot10^5$

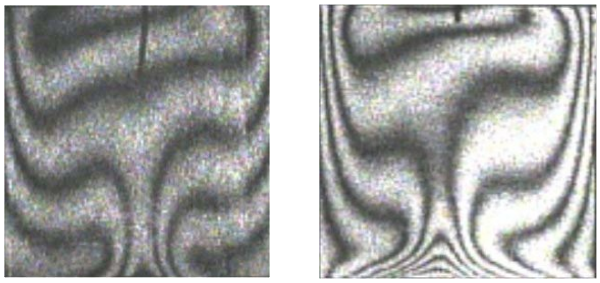

b) $Ra=1.55\cdot10^5$ c) $Ra=1.71\cdot10^5$

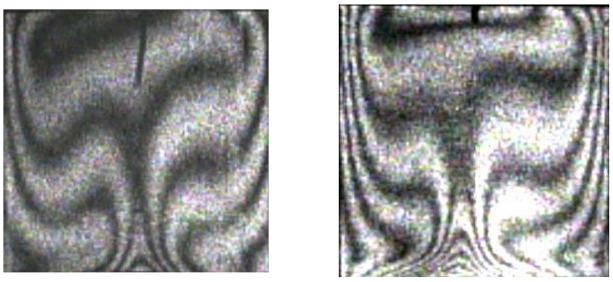

b) $Ra=2.02\cdot10^5$ c) $Ra=1.98\cdot10^5$

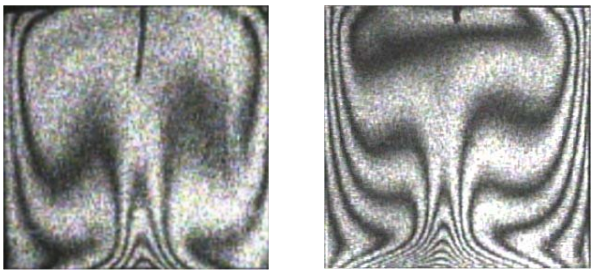

d) $Ra=2.24\cdot10^5$ d) $Ra=2.32\cdot10^5$

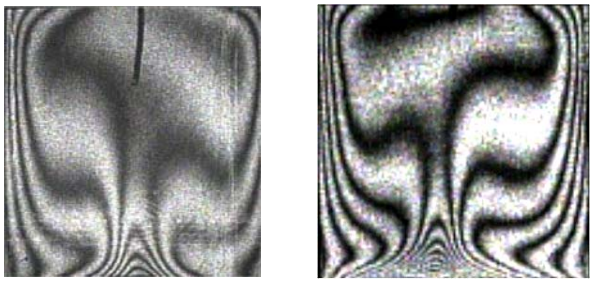

Fig.4 Double exp. Interferograms for $\delta=0.5$

Fig.5 Double exp. Interferograms for $\delta=0.4$

In the interferograms it is visible that the fringes in the high side aren't perpendicular to the surface, from this it points out that the top of the enclosure isn't perfectly adiabatic as before it was presupposed.
Moreover the two configuration show respectively a symmetric and an asymmetric fringes distribution, the raison of this type distribution will be explained afterward.
The experimental analysis is compared with numerical simulation, that permit the extension of the study to a more wide range of Rayleigh number.
In the Fig.6 it is visible the comparison between the double exposure interferograms for the first configuration ($\delta=0,5$) and numerical isotherms for $Ra=2\cdot10^5$, from the comparison emerges that the numerical isotherms follows a behavior analogous to the behavior of the fringes in the double exposure interferogram.

An analogous comparison can be done for the second configuration in the Fig.7, it emerges the same consideration done for the comparison in the Fig.6.

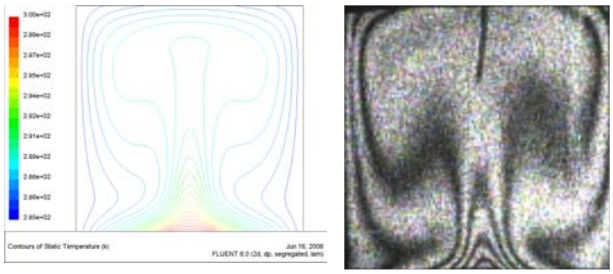

Fig.6 Comparison between Fluent code isotherm for $Ra=2\cdot10^5$ and Double Exposure interferogram for $Ra=2.02\cdot10^5$

In the Fig.8 it is possible to observe a symmetrical distribution of local Nusselt for the configuration with the heat stripe put centrally; the distribution in correspondence of the boundary presents an increase of local Nusselt number caused, as it is visible in the Fig.9, by the air movement, that designs two symmetric counter-rotating cells.

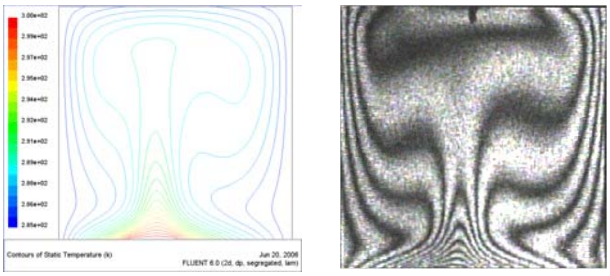

Fig.7 Comparison between Fluent code isotherm for $Ra=2\cdot10^5$ and Double Exposure interferogram for $Ra=1.98\cdot10^5$

The air displacement is due to the continuous heating of the heat source, that moves air toward lateral walls, that, at the same time, make cold the fluid pushing it down and creating the rotation of the two recirculations zones.
The local Nusselt distribution for the configuration with $\delta=0.4$, shown in the Fig.10, has a more consistent increase in the decentralized zone.
The reason of this distribution is the crushing of the left counter rotating cell on the lateral wall due to an asymmetrical position of the heat source.(Fig.11)

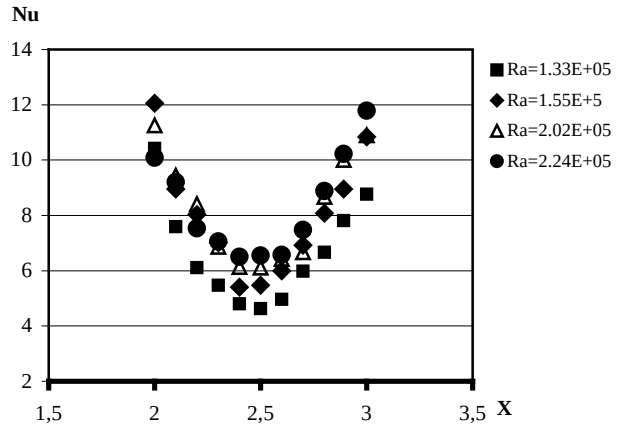


Fig.8 Experimental Local Nusselt for δ=0.5

Fig.9 Streamlines for δ=0.5 ($Ra=2\cdot10^5$)

Moreover between the Fig. 8 and the Fig.10 it is visible a displacement of the minimum in the local Nusselt distribution due to the displacement of the contact line of the two vortexes, because the contact line of two vortexes coincides with the minimum of the local Nusselt distribution.

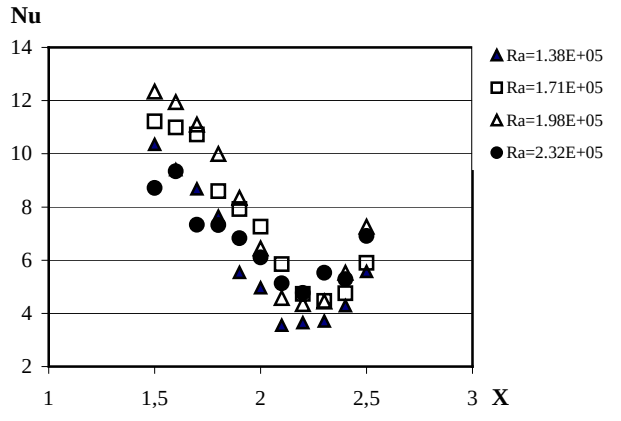


Fig.10 Experimental Local Nusselt for δ=0.4

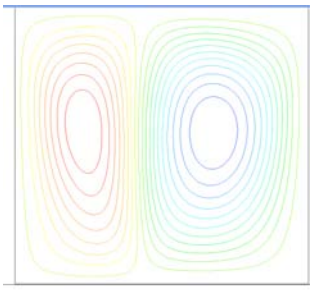

Fig.11 Streamlines for δ=0.4 ($Ra=2\cdot10^5$)

In the Fig.12 it is shown the behavior of average Nusselt number at various Rayleigh numbers for both configurations analyzed.

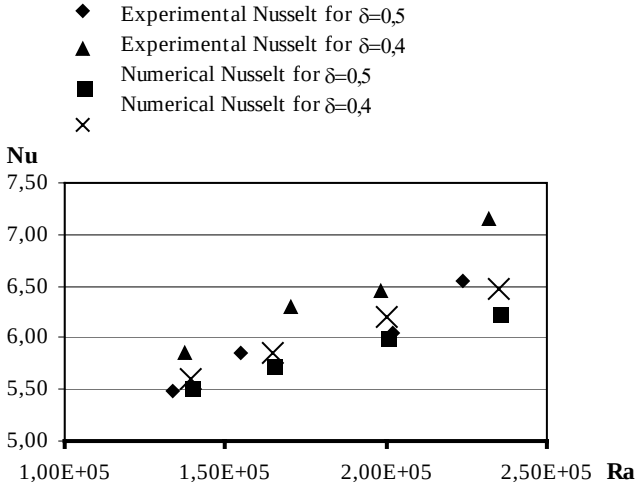


Fig.12 Experimental and numerical $\overline{Nu}_h = f(Ra)$

| δ=0,4 | | | |
|---|---|---|---|
| **Ra** | **Nu (num)** | **Nu (exp)** | **Δ %** |
| 1,38E+05 | 5,551 | 5,859 | 5,546 |
| 1,71E+05 | 5,906 | 6,300 | 6,677 |
| 1,98E+05 | 6,168 | 6,450 | 4,578 |
| 2,32E+05 | 6,449 | 7,150 | 10,871 |

Fig.13 Comparison between the numerical and the experimental average Nusselt number for δ=0.4

It was also elaborated a relation between numerical Nusselt and the correspondent Rayleigh number, with this relation is possible make a comparison between numerical Nusselt and experimental Nusselt at the same value of Rayleigh number and

calculate $\Delta(\%)$, as shown in the Fig.13 and in Fig.14.

| δ=0,5 | | | |
|---|---|---|---|
| **Ra** | **Nu (num)** | **Nu (exp)** | **Δ %** |
| 1,33E+05 | 5,463 | 5,490 | 0,488 |
| 1,55E+05 | 5,657 | 5,850 | 3,303 |
| 2,02E+05 | 6,024 | 6,050 | 0,427 |
| 2,24E+05 | 6,169 | 6,550 | 5,818 |

Fig.14 Comparison between the numerical and the experimental average Nusselt number for $\delta$=0.5.

## 5 Conclusion

In the paper it was analyzed the influence of the heat source position on the natural convective heat transfer in a square cavity.

The analysis was conducted experimentally, with Double Exposure and Real Time interferometry technique for Ra number having a variation range from $1 \cdot 10^5$ to $3 \cdot 10^5$, and numerically by simulation code with Ra number Range of $1 \cdot 10^5 < Ra < 3 \cdot 10^5$.

When the Ra number value increases it is observed a better development of natural convective heat transfer.

The configuration with the heat source put centrally shows a symmetrical development of the phenomenon and therefore a symmetrical distribution of local Nusselt number with an increase of local Nusselt in the boundary of the small heating source due to symmetrical disposition of the two recirculations zones; one of these two vortexes for the second configuration ($\delta$=0.4) is compressed on the lateral wall and that causes an increase on local Nusselt number in the left zone.

*References:*

[1] X1. A. Valencia and R. L. Frederick, Heat transfer in square cavities with partially active vertical walls, *Int. J. Heat Mass Trans.*, Vol.32, No.8, 1989, pp. 1567-1574.

[2] X1. O. Aydin and W. J. Yang, Natural convection in enclosures with localized heating from below and symmetrical cooling from sides, *Int. J. Num .Methods Heat Fluid Flow*, *V*ol.10, No. 5, 2000, pp. 519-529.

[3] X1. E. Ntibarufata, M. Hasnaoui, E. Bilgen and P. Vasseur, Natural convection in partitioned enclosures with localized heating, *Int. J. Num. Meth. Heat Fluid*, Vol.3, No.X, 1993, pp. 133-143.

[4] X1. R. A. V. Ramos and L. F. Milanez, Numerical and experimental analysis of natural convection in cavity heated from below, Proc. 11th IHTC Kyongju, Korea, Vol.3, 1998.

[5] X1. G. Cesini , M. Paroncini, G. Cortella, M. Manzan , Natural convection from a horizontal cylinder in a rectangular cavity, *Int. J. Heat and Mass Transfer*, Vol.42,1999, pp.1801-1811.